



Full waveform inversion in time and frequency domain of velocity modeling in seismic imaging: FWISIMAT a Matlab code

Sagar Singh^a, Ali Ismet Kanli^{b*}, Sagarika Mukhopadhyay^a

^aDepartment of Earth Sciences, Indian Institute of Technology Roorkee, 247667, Roorkee, India.

^{b*} Istanbul University-Cerrahpasa, Faculty of Engineering,

Department of Geophysical Engineering, 34320 Avclar Campus, Istanbul-Turkey E-mail: kanli@istanbul.edu.tr

ABSTRACT

This paper investigates the capability of acoustic Full Waveform Inversion (FWI) in building Marmousi velocity model, in time and frequency domain. FWI is an iterative minimization of misfit between observed and calculated data which is generally solved in three segments, i.e., forward modeling, which numerically solves the wave equation with an initial model, gradient computation of the objective function, and updating the model parameters, with a valid optimization method. FWI codes developed in MATLAB herein FWISIMAT (Full Waveform Inversion in Seismic Imaging using MATLAB) are successfully implemented using the Marmousi velocity model as the true model. An initial model is obtained by smoothing the true model to initiate FWI procedure. Smoothing ensures an adequate starting model for FWI, as the FWI procedure is known to be sensitive on the starting model. The final model is compared with the true model to review the amount of recovered velocities.

Keywords: Seismic Imaging, Full-Waveform Inversion, Acoustic Wave Equation, Gaussian Smoother, Marmousi Velocity Model.

Inversión de onda completa en el campo de frecuencia y tiempo del modelo de velocidad en imágenes sísmicas: el código Matlab FWISIMAT

RESUMEN

Este trabajo investiga la capacidad de la Inversión de Onda Completa (FWI, del inglés Full Waveform inversion) en la construcción del modelo de velocidad Marmousi, en el campo de frecuencia y tiempo. La Inversión de Onda Completa es una minimización repetitiva compleja entre la información observada y la calculada que generalmente se resuelve en tres segmentos: modelado directo, que numéricamente resuelve la ecuación de onda con un modelo inicial; la computación de gradiente de la función objetivo, y la actualización de los parámetros del modelo, con un método de optimización válido. Los códigos de la Inversión de Onda Completa desarrollados en Matlab (FWISIMAT) fueron implementados exitosamente con el modelo de velocidad Marmousi como modelo verdadero. Se obtuvo un modelo inicial tras igualar el modelo verdadero para iniciar el procedimiento de Inversión de Onda Completa. La igualación asegura un modelo inicial adecuado para la Inversión de Onda Completa, mientras que este procedimiento se reconoce por ser sensitivo al modelo inicial. El modelo final se compara con el modelo verdadero para revisar el número de velocidades recuperadas.

Palabras clave: Imagen sísmica; Inversión de Onda Completa; Ecuación de Onda Acústica; Modelo de Velocidad Marmousi; Desenfoque Gaussiano.

Record

Manuscript received: 18/08/2017

Accepted for publication: 29/06/2018

How to cite item

Singh, S., Kanli, A. I., & Mukhopadhyay, S. (2018). Full waveform inversion in time and frequency domain of velocity modeling in seismic imaging: FWISIMAT a Matlab code. *Earth Sciences Research Journal*, 22(4), 291-300.

DOI: <https://doi.org/10.15446/esrj.v22n4.59640>

1. Introduction

Exploration industries commonly use seismic imaging tools, which allow waves to propagate through subsurface rock structure and reveal possible crude oil and natural gas bearing formations. First arrival travel-time tomography is a classical seismic imaging method that for many years has proven to be stable, gives good results, even in lateral heterogeneous media (Chabert, 2010). The data set for the inversion is small (consisting only first arrival travel times), so the method is fast and efficient. However, the first arrival travel times are only sensitive to the long wavelengths of the medium (Chabert, 2010) which limits the possible resolution of the final estimated model. Another disadvantage of the method is the picking of the first arrivals from the seismic data, which is both time consuming, and introduces the possibility of picking errors (Improta et al., 2002). On the other hand, FWI, uses amplitude, travel time and phase information simultaneously to invert the model parameters. FWI is an inverse method that generally employ the least squares objective function to minimize the difference between observed seismic data and synthetic seismic gathers by updating the initial model parameters until convergence (Margrave et al., 2011). The model updates are generated by reverse time migration of the data residual.

The main obstacles that have prevented FWI's common application in exploration seismology are its computational cost and need for a good initial model (Ma, 2010). Various efforts from different perspectives have been developed to reduce the computational costs associated with gradient computation and seismic data generation. For example, Sirgue and Pratt (2004) and Operto et al. (2007) limited the number of frequencies in updating the model. Vigh and Starr (2008) used plane wave method for three-dimensional problems and Margrave et al. (2010) used Phase Shift Plus Interpolation one-way wave gradient calculations.

In this study, FWISIMAT is developed in both time and frequency domain based on acoustic wave equation. The frequency-domain inversion approach is equivalent to the time-domain inversion approach if all of the frequency data components are used in the inversion process (Hu et al., 2009). FWISIMAT use Non-Linear Conjugate Gradient (NLCG) (Dai and Yuan, 1999; Hanger and Zhang, 2005) and Broyden-Fletcher-Goldfarb-Shanno (BFGS) optimization procedure in time and frequency domain algorithms respectively. As to the forward modelling, second order finite difference method is employed due to its high efficiency. This discretization scheme includes absorbing boundary conditions applied on the edges of the velocity medium. However, in order to initiate any iterative scheme an initial model is required (Kanli, 2009), and is derived from smoothing the true velocity model using a Gaussian kernel.

2. FWISIMAT for Time Domain

Full Waveform Inversion is an iterative minimization technique to update the initial model parameters, which is described at k th iteration as follows:

$$\mathbf{m}_{k+1} = \mathbf{m}_k + \alpha_k \mathbf{P}_k \quad (1)$$

where, \mathbf{m} is the model parameter, \mathbf{P} is the direction of update and α is the step length.

FWI is composed of forward modelling computation, gradient computation, and valid optimization technique (Cao and Liao, 2013)

2.1 Forward Modelling

Forward modelling is a necessary step for solving any inverse problem. The governing equation for time domain FWI is non-homogeneous 2D acoustic wave equation (Eq. 2).

$$\frac{1}{v(x,z)^2} \frac{\partial^2 \mathbf{u}(x,z,t)}{\partial t^2} - \nabla^2 \mathbf{u}(x,z,t) = \mathbf{f}(t) \delta(x-x_s) \delta(z-z_s) \quad (2)$$

In Equation 2, $\mathbf{u}(x, z, t)$ is the source wave-field, $v(x, z, t)$ is the velocity, $\mathbf{f}(t)$ is the source time function and (x_s, z_s) is the source location in space.

Let $\mathbf{u}_{n,m}^l$ be the wave-field at the time $l\Delta t$ and spatial position $(n\Delta x, m\Delta z)$, $v_{n,m}$ be the velocity at $(n\Delta x, m\Delta z)$ then Equation 2 can be discretized using central difference scheme as follows:

$$\mathbf{u}_{n,m}^{l+1} = 2\mathbf{u}_{n,m}^l - \mathbf{u}_{n,m}^{l-1} + \frac{\Delta t^2}{\Delta v_{n,m}^2} \left(\frac{\mathbf{u}_{n+1,m}^l - 2\mathbf{u}_{n,m}^l + \mathbf{u}_{n-1,m}^l}{\Delta x^2} + \frac{\mathbf{u}_{n,m+1}^l - 2\mathbf{u}_{n,m}^l + \mathbf{u}_{n,m-1}^l}{\Delta z^2} \right) + \mathbf{f}(l\Delta t) \delta(n-n_s) \delta(m-m_s) \quad (3)$$

with the initial conditions

$$\mathbf{u}_{n,m}^{-1} = 0, \mathbf{u}_{n,m}^0 = 0 \quad (4)$$

The numerical stability conditions for Equations 3 and 4 is as follows:

$$\Delta t \leq \sqrt{\frac{1}{2} \frac{\min(\Delta x, \Delta z)}{v_{max}}} \quad (5)$$

The unsuitable choice of time and spatial steps may cause severe dispersion and wave distortion in wave simulation. In order to suppress numerical dispersion, it is usually required that there are 10 sampling points per wavelength in Equation 2,

$$\min(\Delta x, \Delta z) < \frac{v_{min}}{10 f_{max}} \quad (6)$$

For the same frequency, the numerical dispersion increases as the spatial steps increase. However, the dispersion can be depressed if the higher point approximation schemes are used.

In numerical computations, the computational domain is usually truncated to a finite region. So, absorbing boundary conditions (ABCs) are included in order to reduce reflection from the edges of the grid. The absorbing boundary conditions are constructed from paraxial approximations of the wave equation (Clayton and Enquist, 1977). Figure 1 illustrates the effect of boundary conditions when the wave-field hits the edges of the medium. Wave-fields are recorded for each time at each receiver positions per source. These records are called as synthetic seismograms (Fig. 2).

2.2 Gradient Computation: Reverse Time Migration

The objective function ($\mathcal{O}(\mathbf{v})$) that would be minimized is given as follows:

$$\mathcal{O}(\mathbf{v}) = \frac{1}{2} \mathbf{d}_{obs} - \mathbf{d}_{cal}^2 \quad (7)$$

where, \mathbf{d}_{obs} is the observed data and \mathbf{d}_{cal} is the calculated data. The gradient of the objective function is given as follows:

$$\nabla \mathcal{O}(\mathbf{v}_0) = - \sum_s \int_0^T \mathbf{q}_s(x, z, t) \partial_{tt} \mathbf{u}_{0,s}(x, z, t) dt \quad (8)$$

where, \mathbf{q}_s represents the back-propagated wave-field from receivers to source. \mathbf{q}_s can be computed from Equation 9 backward in time (Demant, 2015).

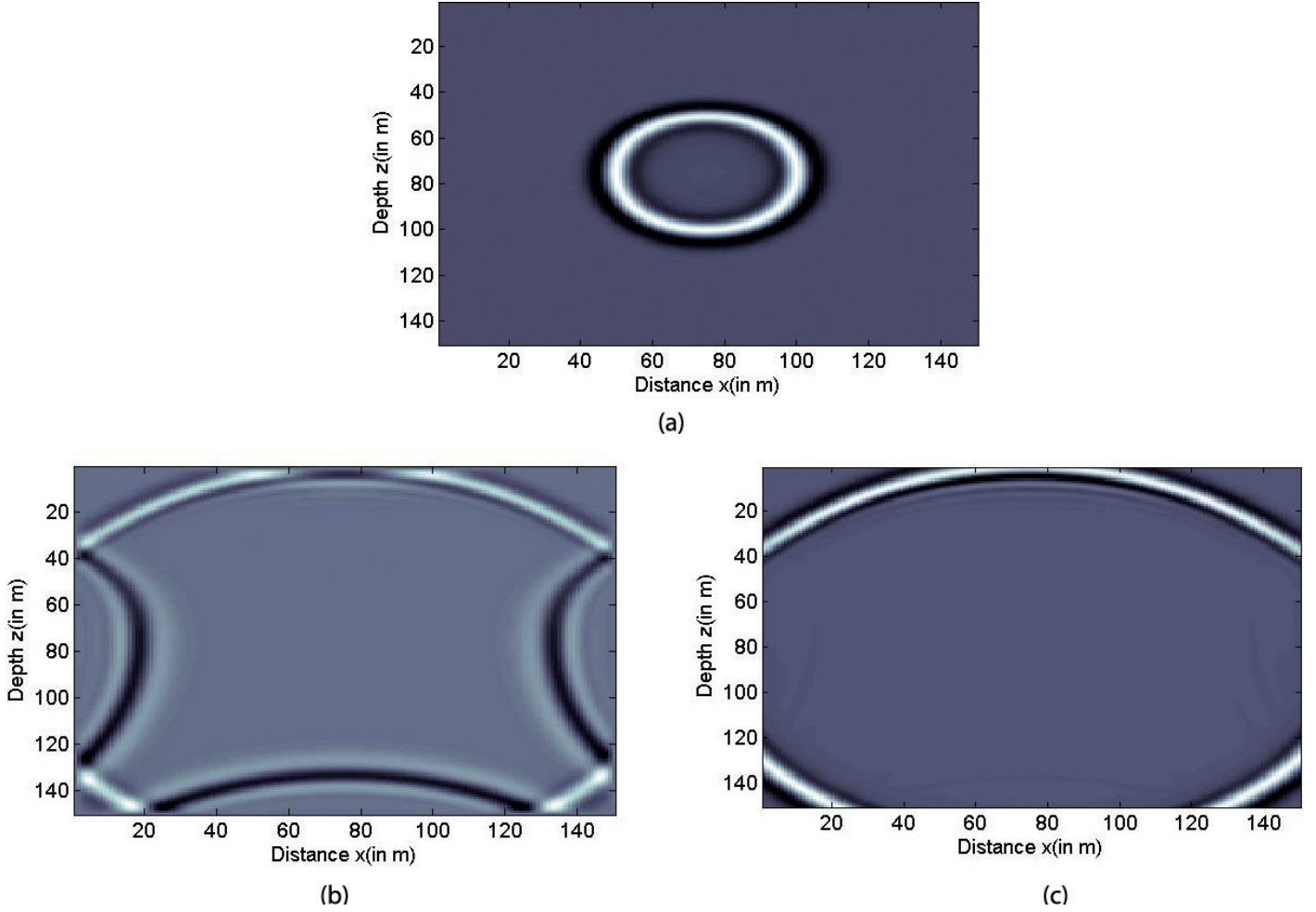


Figure 1. Effect of boundary conditions. (a) Wave-field at time 0.17 sec., (b) wave-field at time $t = 0.42$ sec (no boundary condition is used), (c) wave-field at time $t = 0.42$ sec (absorbing boundary conditions is used).

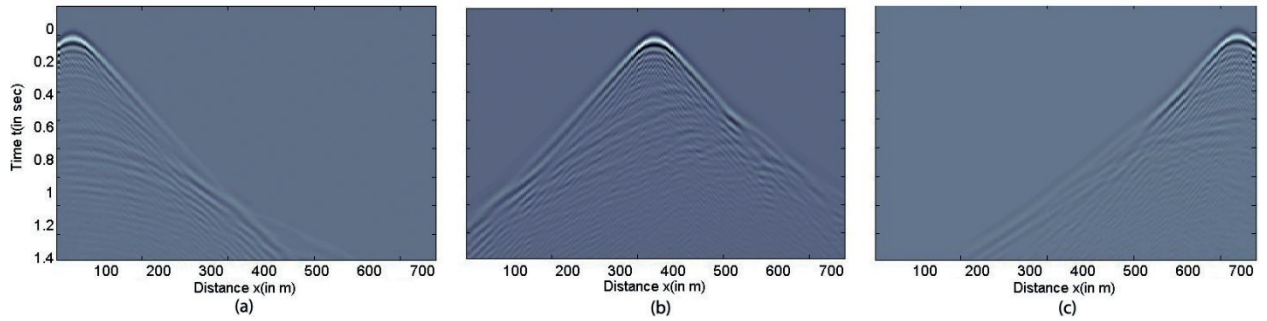


Figure 2. Synthetic shot data for true model at shot location (a) $x=50$ -m (b) $x=360$ -m (c) $x=670$ -m.

$$\left(\frac{1}{\mathbf{v}_0(x,z)^2} \frac{\partial^2}{\partial t^2} - \nabla^2 \right) \mathbf{q}_s(x,z,t) = \mathbf{r}_s(x,t) \quad (9)$$

In Equation 9, \mathbf{r} is the residual field (Eq. 10).

$$\mathbf{r}(x,t) = \mathbf{d}_{obs}(x,t) - \mathbf{d}_{cal}(x,t) \quad (10)$$

The sum over \mathbf{r} in Equation 10 is sometimes called a *stack* (Fig. 3). Stack uses the redundancy in the data to bring out the information and reveal more details (Demantet, 2015).

A systematic way for solving back-propagated wave-field (Eq. 9) is to follow the following sequence of three steps: (1) time reverse the data residual $\mathbf{r}(x,t)$ at each receiver position, (2) solve the wave equation forward in time with this new right hand side, and (3) time reverse the result at each receiver position in x .

2.3 Optimization: Non-Linear Conjugate Gradient Method

Conjugate gradient optimization method updates the velocity model according to the descent direction \mathbf{P}_k (Eq. 11).

$$\mathbf{v}_{k+1} = \mathbf{v}_k + \alpha_k \mathbf{P}_k \quad (11)$$

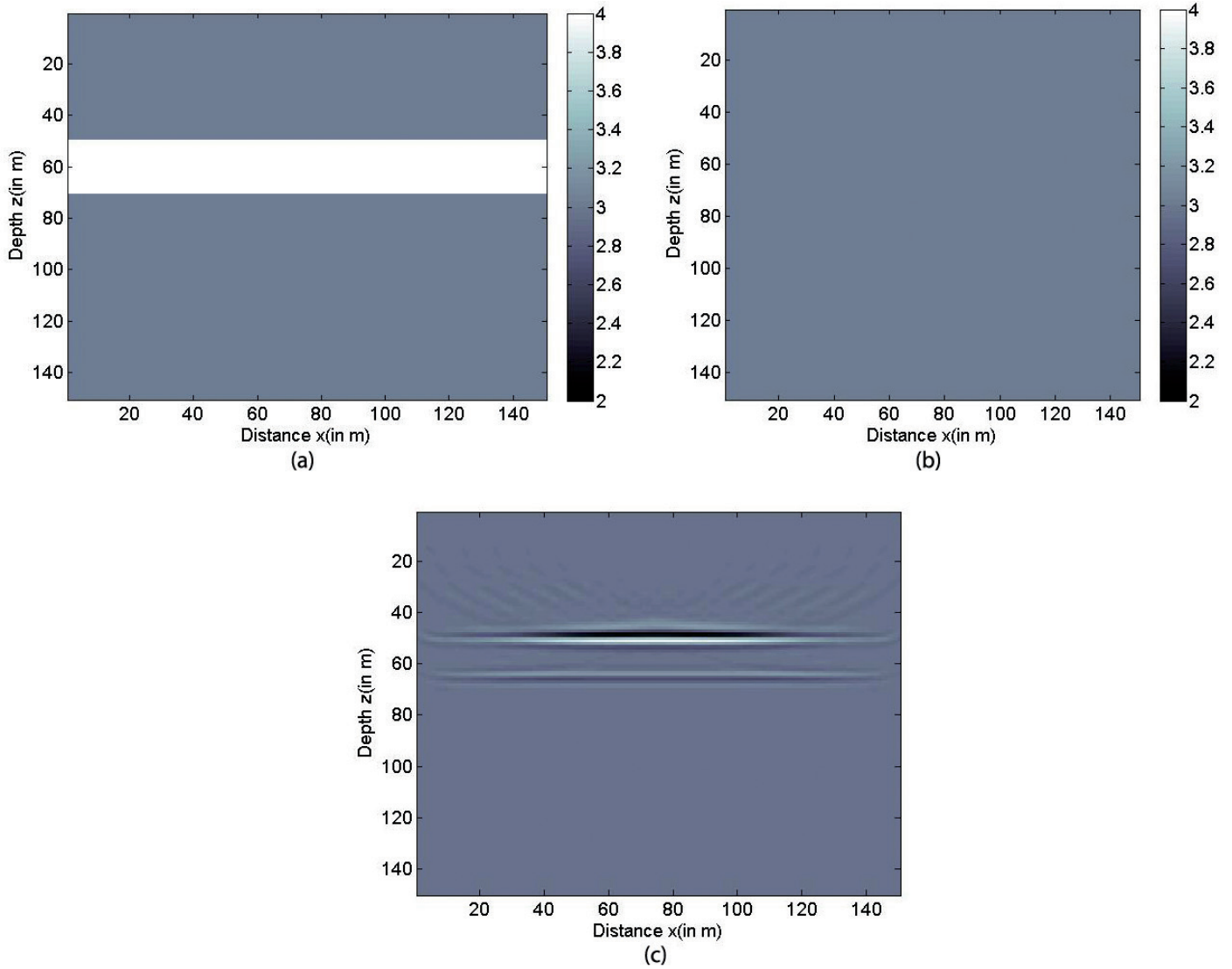


Figure 3. An example of gradient computation using reverse time migration method, where (a) is a theoretical model (b) is initial model and (c) is migrated image.

According to Pica et al., (1990) step length is estimated as follows:

$$\alpha_k = \frac{\mathbf{J}_k \mathbf{P}_k \cdot \mathbf{d}_{obs} - \mathbf{d}_{cal}}{\mathbf{J}_k \mathbf{P}_k \cdot \mathbf{J}_k \mathbf{P}_k} \quad (12)$$

where, \mathbf{J}_k stands for Jacobian matrix and $\langle \cdot, \cdot \rangle$ denotes inner product.

For computing the direction \mathbf{P}_k , NLCG optimization process is used (Hanger and Zhang, 2005), which decreases the objective function along the conjugate gradient direction (Eq. 13).

$$\mathbf{P}_k = \begin{cases} -\nabla O(\mathbf{v}_0), & k=1 \\ -\nabla O(\mathbf{v}_k) + \gamma_k \mathbf{P}_{k-1} & k > 1 \end{cases} \quad (13)$$

In Equation 13, γ_k is computed according to Equation 14

$$\gamma_k = \max\left(0, \min\left(\gamma_k^{HS}, \gamma_k^{DY}\right)\right) \quad (14)$$

in which

$$\begin{cases} \gamma_k^{HS} = \frac{\langle \nabla O(\mathbf{v}_k), \nabla O(\mathbf{v}_k) - \nabla O(\mathbf{v}_{k-1}) \rangle}{\langle \mathbf{P}_{k-1}, \nabla O(\mathbf{v}_k) - \nabla O(\mathbf{v}_{k-1}) \rangle} \\ \gamma_k^{DY} = \frac{\langle \nabla O(\mathbf{v}_k), \nabla O(\mathbf{v}_k) \rangle}{\langle \mathbf{P}_{k-1}, \nabla O(\mathbf{v}_k) - \nabla O(\mathbf{v}_{k-1}) \rangle} \end{cases} \quad (15)$$

This provides an automatic direction reset while over-correction of γ_k in conjugate gradient iterations. It reduces to steepest descent method when the subsequent search directions lose conjugacy.

2.4 Numerical Computation: Marmousi Velocity Model

The Marmousi Velocity model is a benchmark model for testing the ability of migration or inversion methods (Zhang, 2009). The original velocity model is shown in Figure 4. However, for this study a resampled velocity model (true velocity model) is used as illustrated in Figure 5.

The Initial model is generated by smoothing the true model using a Gaussian kernel (Fig. 6).

There were total 31 sources at a depth of 10-m and 720 receivers at a depth of 2-m equally spaced in the medium. Absorbing boundary condition

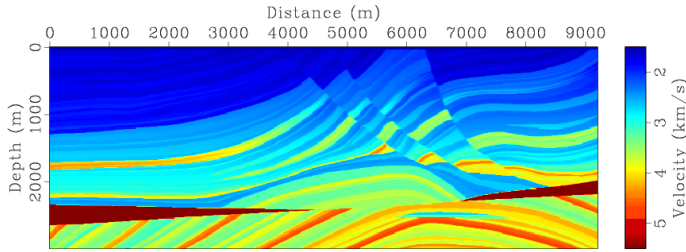


Figure 4. Original Marmousi model.

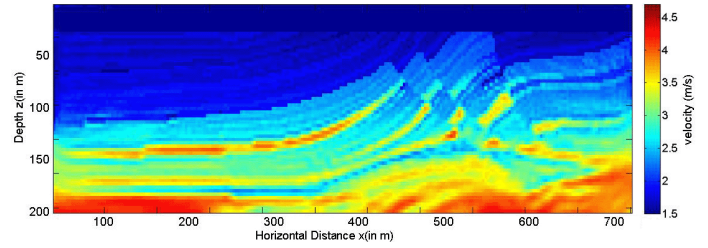


Figure 7. Inversion result after 200 iteration

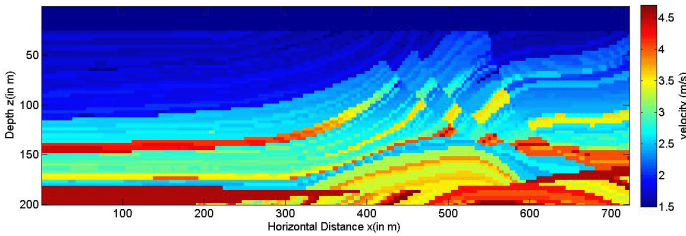


Figure 5. True model.

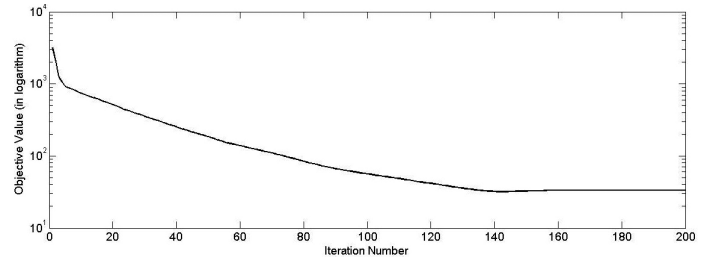


Figure 8. Objective function value in logarithmic scale at each iteration.

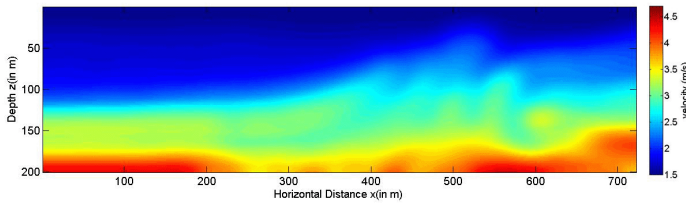


Figure 6. Initial Velocity model for inversion

is applied over all four edges of the medium. Grid spacing is kept at $\Delta x (= \Delta z) = 0.01$ -m, sampling is taken over $\Delta t = 0.0014$ with number of sample point set as $Nt=890$. To save computational, we use the whole frequency band (0-20Hz) for the inversion (in frequency domain, this implementation is different). In practice, multiscaling approach is employed to reconstruct the model from low to high frequency fashion (as discussed later in the paper). This implementation generally cause the difference of the resolution in different inversion algorithms. However, the time-domain FWI is still able to provide good estimation of the acoustic parameter without sacrificing the high resolution. Figure 7 and Figure 8 represent the inversion result after 200 iterations and the value of the objective function after each iteration.

A more qualified analysis of the velocities is easier when looking at the velocity profiles in Fig. 9. Velocity logs at three different locations are extracted (at 200, 400 and 600 m) from true, initial and final model. In all three logs, the final velocities from FWI result matches with the true velocities very well.

3. FWISIMAT in Frequency Domain

Frequency domain Waveform Inversion, which includes solving the wave equation forward modelling and inversion, is similar to time domain waveform inversion. The efficiency of frequency domain FWI depends on the number of frequencies used for the inversion and is independent of the number of sources used for inversion.

3.1 ForwardModelling

For frequency domain forward modelling Equation 2 must be converted into frequency domain (Eq. 16).

$$\frac{\omega^2}{v(x,z)^2} \mathbf{u}(x,z,\omega) + \nabla^2 \mathbf{u}(x,z,\omega) = \mathbf{s}(x,z,\omega) \quad (16)$$

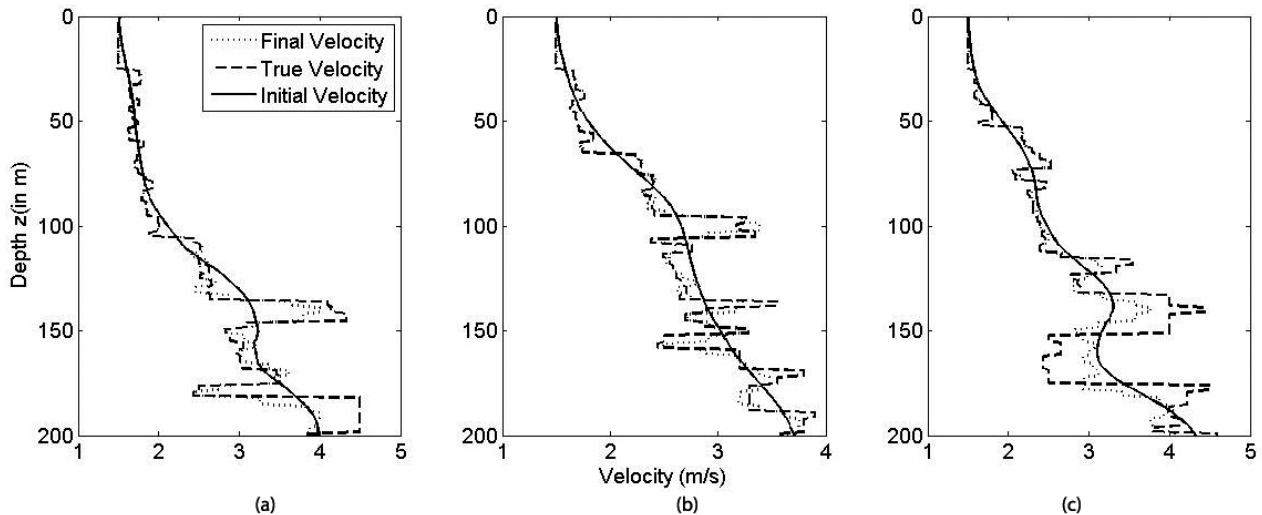


Figure 9. Velocity log extracted at horizontal distance $x =$ (a) 200 m (b) 400 m (c) 600 m

In Equation 16, ω is the frequency, $\mathbf{v}(x, z)$ is the velocity in the medium, $\mathbf{u}(x, z, \omega)$ is the source wave-field, and $\mathbf{s}(x, z, \omega)$ is source in frequency domain (Fourier-transform of time-domain source wavelet). The boundary condition in frequency domain is given as follows:

$$\frac{\partial \mathbf{u}}{\partial \mathbf{n}} - ih(x, y) \mathbf{u} = 0 \tag{17}$$

where, \mathbf{n} is the outward normal of the boundary, $h = \omega / \mathbf{v}(x, z)$, and i is the imaginary unit (Erlangga, 2008; Zhang and Dai, 2013). By means of the finite difference technology along with the boundary condition, the wave equation (Eq. 16 and 17) can be recast into matrix form as follows:

$$A \mathbf{u} = \mathbf{s} \tag{18}$$

In Equation 18, A is a complex-valued, $n_x \times n_z$ (discretization along xx and z direction) order impedance matrix and it depends on frequency, medium properties, finite difference format, and boundary conditions (Wang et al., 2012). Solving the linear system in Equation 18 wave-field can be obtained (Fig. 10). Wave-fields are recorded for each frequency at each receiver positions per source. In FWISIMAT the above mentioned process is implemented as follows:

$$D = \mathbf{r}'^* (A \setminus Q) \tag{19}$$

In Equation 19, $D (= \mathbf{d}_{cal})$, \setminus is the matrix inversion operator and \mathbf{r}' is the transpose of the vector consisting receivers at spatial positions and Q is the source vector. Figure 11 illustrate the data obtained from a same source but for different frequencies.

3.2 Gradient Computation: Reverse Time Migration

The gradient of the objective function in frequency domain is given as follows,

$$\nabla O(\mathbf{v}_0) = -2\pi \int_R \widehat{q}_s(x, z, \omega) \omega^2 \overline{\widehat{u}_{0,s}(x, z, \omega)} d\omega \tag{20}$$

where, $\overline{\widehat{u}_{0,s}(x, z, \omega)}$ represent the complex conjugate operator (Demant, 2015). The integral in ω in above equation is over R and should be truncated to the number of frequencies used in the process. Equation 20 represents the frequency domain version of Equation 10. In FWISIMAT the back-propagated wave-field $\widehat{q}_s(x, z, \omega)$ is computed as follows:

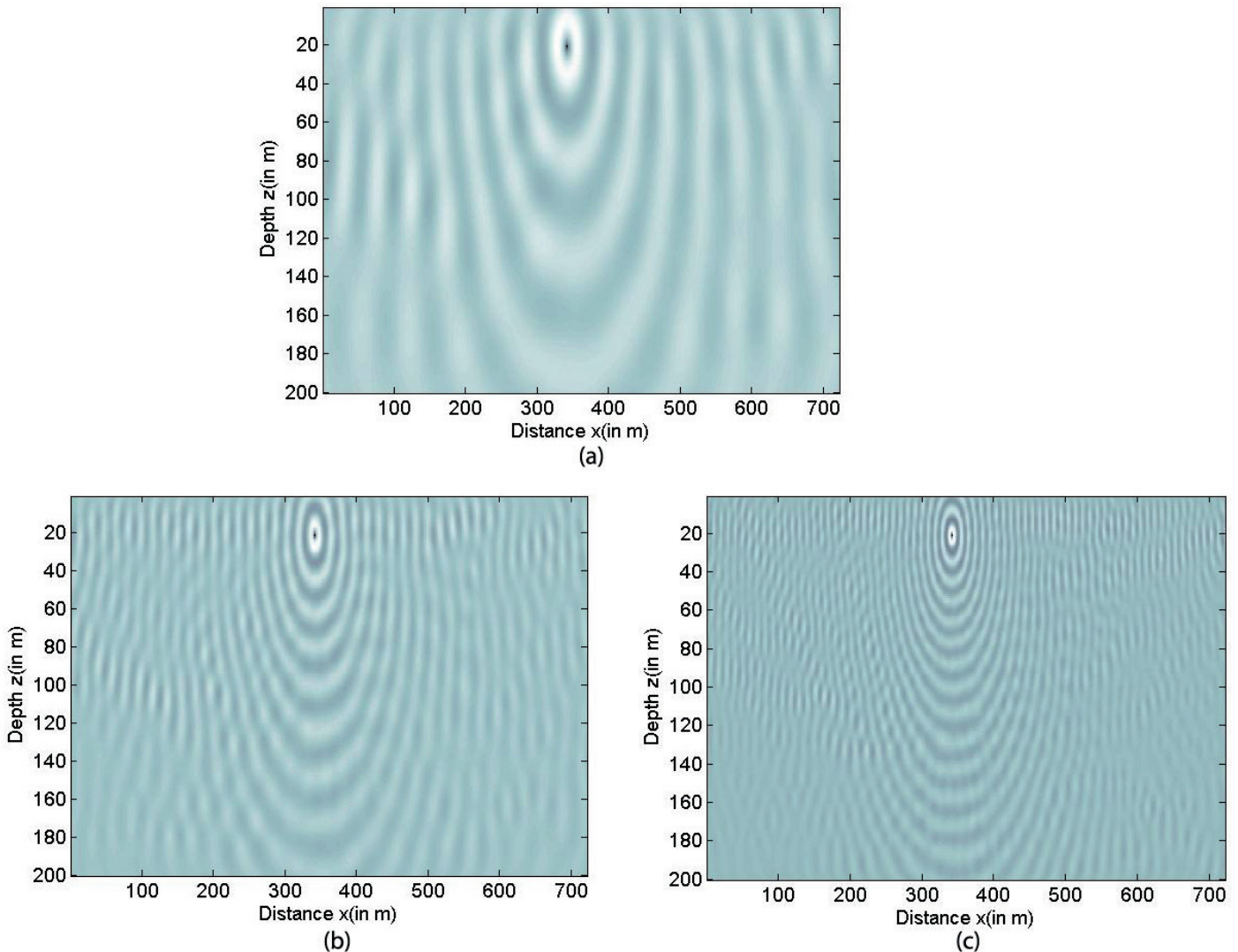


Figure 10. Wave-field recorded at frequency (a) 5 Hz (b) 12 Hz (c) 20 Hz.

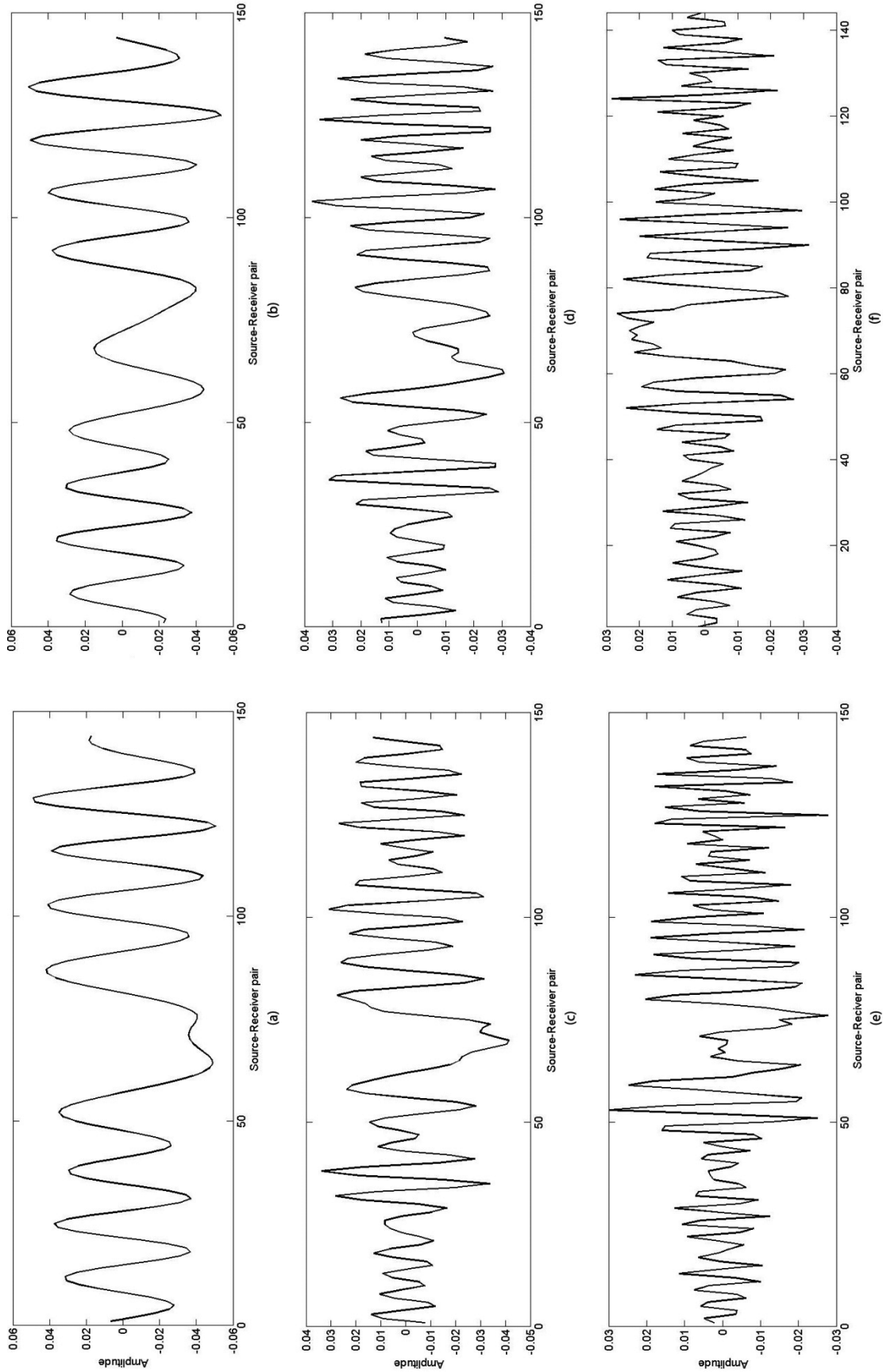


Figure 11. Frequency data for true model at, (a) 5 Hz frequency component, real (b) 5 Hz frequency component, imaginary (c) 12 Hz frequency component, real (d) 12 Hz frequency component, imaginary (e) 20 Hz frequency component, real (f) 20 Hz frequency component, imaginary

$$\mathbf{V} = \mathbf{A}^{-1} \left(\mathbf{r}^* (\mathbf{D}_{\text{obs}} - \mathbf{r}^* (\mathbf{A} \setminus \mathbf{s})) \right) \quad (21)$$

where, $\mathbf{V} (= \widehat{\mathbf{q}_s})$ is back-propagated wave-field. \mathbf{D}_{obs} can be obtained from Equation 19 if applied on true model.

3.3 Optimization: Broyden-Fletcher-Goldfarb-Shanno (BFGS)

In time domain FWI, NLCG optimization method is used. NLCG consumes a substantial time to converge. According to Zhang and Luo (2013), the BFGS based method has higher inversion accuracy and converge faster than the conjugate gradient based algorithm because the later uses the second order derivative information in computation.

The BFGS method is a quasi-Newton method which proposed dependently by Broyden (1970), Fletcher (1970), Goldfarb (1970), Shanno (1970). Let \mathbf{H}_k is the inverse hessian approximation then the next iterate will be given as follows:

$$\mathbf{H}_{k+1} = \mathbf{H}_k + \frac{\mathbf{b}\mathbf{b}^T}{\mathbf{g}_k^T \mathbf{b}} \left[\frac{\mathbf{g}_k^T \mathbf{H}_k \mathbf{g}_k}{\mathbf{g}_k^T \mathbf{b}} + 1 \right] - \frac{1}{\mathbf{g}_k^T \mathbf{b}} \left[\mathbf{b}\mathbf{g}_k^T \mathbf{H}_k + \mathbf{H}_k \mathbf{g}_k \mathbf{b}^T \right] \quad (22)$$

where, $\mathbf{b}_k = \mathbf{m}_{k+1} - \mathbf{m}_k$ and $\mathbf{g}_k = \nabla O(\mathbf{m}_{k+1}) - \nabla O(\mathbf{m}_k)$. For $k = 1$, \mathbf{H}_1 can be approximated by an identity matrix. The next update on the model parameter is given as follows:

$$\mathbf{m}_{k+1} = \mathbf{m}_k + \alpha_k \mathbf{P}_k \quad (23)$$

where,

$$\mathbf{P}_k = \begin{cases} -\nabla O(\mathbf{v}_0), & k=1 \\ -\mathbf{H}_k \nabla O(\mathbf{v}_k) & k>1 \end{cases} \quad (24)$$

BFGS method does not require exact line search in order to converge, therefore, Wolfe line search algorithm (Wolfe, 1969; 1971) is acquired to find step length α_k . The strong Wolfe line search algorithm requires the following conditions to be satisfied.

$$O(\mathbf{m}_k + \alpha_k \mathbf{P}_k) \leq O(\mathbf{m}_k) + c_1 \alpha_k \nabla O(\mathbf{m}_k)^T \mathbf{P}_k \quad (25)$$

$$\left| \nabla O(\mathbf{m}_k + \alpha_k \mathbf{P}_k)^T \mathbf{P}_k \right| \leq \left| c_2 \nabla O(\mathbf{m}_k)^T \mathbf{P}_k \right| \quad (26)$$

In Equation 26 $0 < c_1 < c_2 < 1$.

3.4 Numerical Computation: Marmousi Velocity Model

True and initial velocity model for frequency domain FWISIMAT are kept same as Figure 5 and Figure 6 respectively (ensuring 10 grid-points per wavelength). The number of sources and receivers are 30 and 90 which are equally spaced in the medium at a depth of 20-m. The absorbing boundary conditions are applied on all edges of the medium. The inversion result after 25 iterations is shown in Figure 12. The inversion is from low to high frequency, and choice of which is usually related to the model. The low frequencies are more linear related to the model perturbations than the high frequencies (Sirgue, 2003). Therefore, the inversion process should start with the low frequency components and progressively add higher frequencies. This will help mitigate some of the non-linearity of the problem, hence increasing the chances of finding the global minimum. It also ensures that progressively higher wavenumbers are recovered (Ravaut et al., 2004).

According to the experience and experiments, twelve frequencies are selected, not only to obtain good results, but also for faster computation. The twelve frequencies from low towards high are 1.00 2.73 4.45 6.18 7.91 9.64 11.36 13.09 14.82 16.55 18.27 20.00. Figure 13 shows the objective function value in logarithmic scale during the inversion process.

Figure 14 shows the velocity comparison among the final, true model and initial model at different horizontal distances. After frequency domain waveform inversion algorithm, the final result is obtained close to the true velocity model, especially that the near-surface speed is almost identical to the theoretical model. The results confirm the validity of the algorithm.

4. Conclusions

The Full Waveform Inversion method and its capabilities, when applied to a complex geological model, have been presented in this study. The FWISIMAT algorithm used in the study, performs an iterative search for a velocity model that minimizes the residuals between the data computed in the velocity model and the observed data, i.e. the final result is a “best fit” model. The whole wave-field, including both waveform and phase, is being used as data. FWISIMAT computes in the time and frequency domain. Comparing with the frequency domain inversion method, the time domain method has the advantage of high efficiency in forward modelling as the wave modelling in frequency domain requires solving a large-scale system at each iteration which is time consuming for large scale problems. Apart from this, time domain modelling provides the most flexible framework to apply time windowing of arbitrary geometry. In the frequency domain, the computational cost is only proportional to the number of frequencies used in the inversion, and not the number of sources. If the seismic data contains wide angle components, there will be a redundancy in the wave number spectrum present in the data, such a redundancy can be exploited in the frequency domain FWI by inverting fewer frequencies (and hence save computational costs) because it is possible to invert for single, discrete frequencies one at the time. Another great advantage with the frequency domain implementation is the ease and efficiency when adding multiple sources. The method is very sensitive to the non-linearity of the problem,

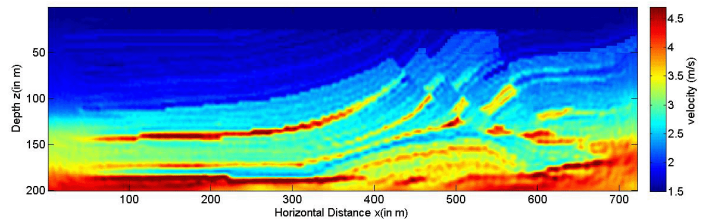


Figure 12. Inversion result

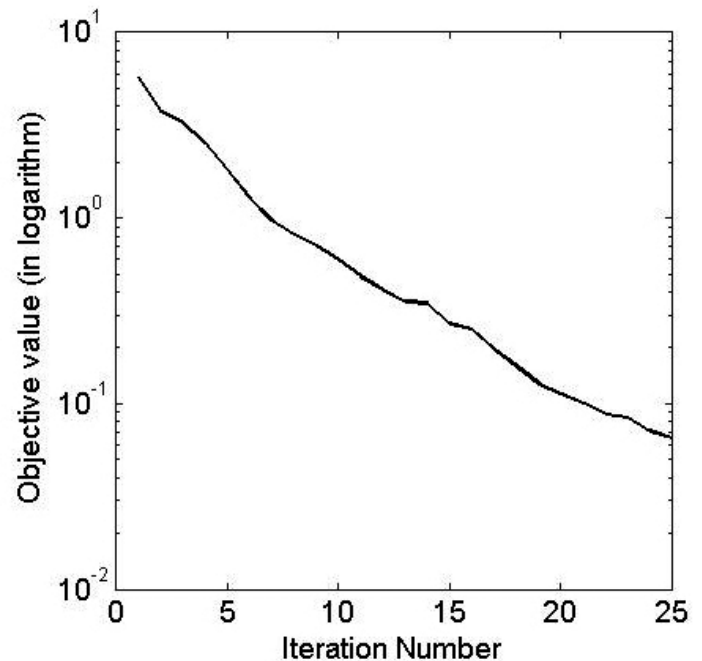


Figure 13. Objective function value in logarithmic scale at each iteration.

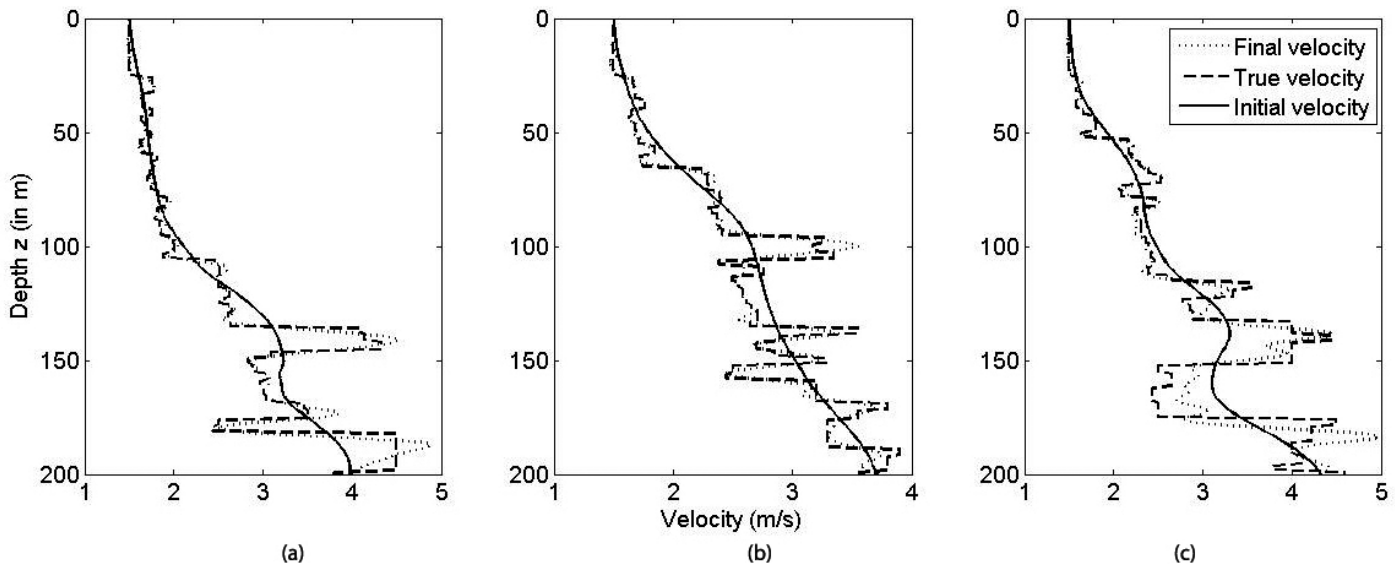


Figure 14. Velocity log extracted at horizontal distance $x =$ (a) 200 m (b) 400 m (c) 600 m

and proper input parameters, such as an accurate starting model and an initial frequency as low as possible, is important for obtaining optimum results. In this work, it is shown that Full Waveform inversion has a great potential for estimating complex velocity models such as Marmousi Velocity Model when the acquisition parameters are as optimal as possible. For the future, applying FWI to real data from more complex geological medium and developing a migration tool and test the effect of FWI on a migrated image, are interesting challenges.

Acknowledgments

This work was supported by the Research Fund of Istanbul University, project number: BEK-2017-27284 The authors thank the anonymous reviewers for their constructive remarks in the preparation of the final form of the paper.

References

- Broyden, C. G. (1970). The Convergence of a Class of Double- Rank Minimization Algorithms. 2. The New Algorithm. *Journal of the Institute of Mathematics and its Applications*, 10, 222-231.
- Chabert, A. (2010). *Seismic imaging of the sedimentary and crustal structure of the hatton basin on the Irish Atlantic margin*. Ph.D. Thesis, University College Dublin, Ireland.
- Clayton, R. & Engquist, B. (1977). Absorbing Boundary Conditions for Acoustic and Elastic Wave Equations. *Bulletin of the Seismological Society of America*, 67(6), 1529-1540.
- Dai, Y. H. & Yuan, Y. (1999). A nonlinear conjugate gradient method with a strong global convergence property. *SIAM Journal on Optimization*, 10(1), 177-182.
- Demant, L. (2015). Waves and Imaging, Class Notes. <http://math.mit.edu/icg/resources/notes325.pdf> (last accessed April 2016).
- Erlangga, Y. A. (2008). Advances in Iterative Methods and Preconditioners for the Helmholtz Equation. *Archives of Computational Methods in Engineering*, 15(1), 37-66.
- Fletcher, R. (1970). A New Approach to Variable Metric Algorithms. *Computer Journal*, 13(3), 317-322.
- Goldfarb, D. (1970). A Family of Variable Metric Methods Derived by Variational Means. *Mathematics of Computation*, 24(109), 23-26.
- Hager, W. W., & Zhang, H. (2006). A survey of nonlinear conjugate gradient methods. *Pacific Journal of Optimization*, 2(6), 35-58.
- Hu, W., Abubakar, A. & Habashy, T. M. (2009). Simultaneous Multifrequency Inversion of Full-waveform Seismic Data. *Geophysics*, 74(2), 1-14.
- Improta, L., Zollo, A., Herrero, Frattini, A., R., Virieux, J. & Dell'Aversana, P. (2002). Seismic imaging of complex structures by non-linear travelttime inversion of dense wide-angle data: application to a thrust belt. *Geophysical Journal International*, 151(1), 264-278.
- Kanli, A. I. (2009). Initial Velocity Model Construction of Seismic Tomography in Near- surface Application. *Journal of Applied Geophysics*, 67(1), 52-62.
- Cao, D. & Liao, W. (2013). *Full Waveform Inversion of crosswell seismic data using automatic differentiation*. GeoConvention Integration, Geoscience Engineering Partnership, Calgary, Canada, May, 6-12.
- Ma, Y. (2010). *Full waveform inversion with image-guided gradient*. M.Sc. Thesis, Center for Wave Phenomena, Colorado School of Mines, Colorado, USA.
- Margrave, G., Ferguson, R. & Hogan, C. (2010). Full waveform inversion with wave equation migration and well control. *CREWES Research Report*, 22(63), 1-20.
- Margrave, G., Yedlin, M. & Innanen, K. (2011). Full waveform inversion and the inverse hessian. *CREWES Research Report*, 23(77), 1-13.
- Operto, S., Virieux, J., Amestoy, P., L'Excellent, J. Y., Giraud, L. & Ben-Hadj-Ali, H. (2007). 3D finite-difference frequency-domain modeling of visco-acoustic wave propagation using a massively parallel direct solver: A feasibility study. *Geophysics*, 72(5), 195-211.
- Pica, A., Diet, J. P. & Tarantola, A. (1990). Nonlinear inversion of seismic reflection data in a laterally invariant medium. *Geophysics*, 55(3), 284-292.
- Ravaut, C., Operto, S., Improta, L., Virieux, J., Herrero, A. & Dell'Aversana, P. (2004). Multiscale imaging of complex structures from multifold wide-aperture seismic data by frequency-domain full-waveform tomography: application to a thrust belt. *Geophysical Journal International*, 159(3), 1032-1056.
- Shanno, D. F. (1970). Conditioning of Quasi-Newton Methods for Function Minimization. *Mathematics of Computation*, 24(111), 647-656.
- Sirgue, L. (2003). *Frequency domain waveform inversion of large offset seismic data*. Ph.D Thesis, l'Ecole Normale Supérieure de Paris, Paris, France.
- Sirgue, L. & Pratt, R. G. (2004). Efficient waveform inversion and imaging: A strategy for selecting temporal frequencies. *Geophysics*, 69(1), 231-248.
- Vigh, D. & Starr, W. (2008). 3D pre-stack plane-wave, full-waveform inversion. *Geophysics*, 73(5), 135-144.

- Wang, M., Zhang, D., Yao, D., Qin, Q., & Xu, L. (2012). Application of Frequency-Domain Waveform Inversion Method in Marmousi Shots Data. *Wuhan University Journal of Natural Sciences*, 17(4), 326-330.
- Wolfe, P. (1969). Convergence Conditions for Ascent Methods. *SIAM Review*, 11(2), 226-235.
- Wolfe, P. (1971). Convergence Conditions for Ascent Methods II: Some Corrections. *SIAM Review*, 13(2), 185-188.
- Zhang, W. & Luo, J. (2013). Full-waveform Velocity Inversion Based on the Acoustic Wave Equation. *American Journal of Computational Mathematics*, 3(3B), 13-20.
- Zhang, W. (2009). *Imaging Methods and Computations Based on the Wave Equation*. Beijing, Science Press.
- Zhang, W. & Dai, Y. (2013). Finite-Difference Solution of the Helmholtz Equation Based on Two Domain Decomposition Algorithm. *Journal of Applied Mathematics and Physics*, 1(4), 18-24.